

UC San Diego

UC San Diego Previously Published Works

Title

Dynamics of stimulated L → H transitions

Permalink

<https://escholarship.org/uc/item/1hf5847q>

Journal

Physics of Plasmas, 20(8)

ISSN

1070-664X

Authors

Miki, K
Diamond, PH
Hahn, S-H
[et al.](#)

Publication Date

2013-08-01

DOI

10.1063/1.4818429

Copyright Information

This work is made available under the terms of a Creative Commons Attribution-NonCommercial-NoDerivatives License, available at <https://creativecommons.org/licenses/by-nc-nd/4.0/>

Peer reviewed

Dynamics of stimulated L H transitions

K. Miki, P. H. Diamond, S.-H. Hahn, W. W. Xiao, Ö. D. Gürcan, and G. R. Tynan

Citation: *Physics of Plasmas* (1994-present) **20**, 082304 (2013); doi: 10.1063/1.4818429

View online: <http://dx.doi.org/10.1063/1.4818429>

View Table of Contents: <http://scitation.aip.org/content/aip/journal/pop/20/8?ver=pdfcov>

Published by the [AIP Publishing](#)



Re-register for Table of Content Alerts

Create a profile.



Sign up today!



Dynamics of stimulated $L \rightarrow H$ transitions

K. Miki,^{1,2} P. H. Diamond,^{1,3} S.-H. Hahn,⁴ W. W. Xiao,^{1,3} Ö. D. Gürçan,⁵ and G. R. Tynan³

¹WCI Center for Fusion Theory, National Fusion Research Institute, Daejeon 305-333, South Korea

²Center for Computational Science and e-Systems, Japan Atomic Energy Agency, Chiba 277-8587, Japan

³Center for Momentum Transport and Flow Organization, University of California, San Diego, California 92093, USA

⁴KSTAR Team, National Fusion Research Institute, Daejeon 305-333, South Korea

⁵LPP, Ecole Polytechnique, CNRS, 92118 Palaiseau Cedex, France

(Received 26 March 2013; accepted 26 July 2013; published online 15 August 2013)

We report on model studies of stimulated $L \rightarrow H$ transitions [K. Miki *et al.*, Phys. Rev. Lett. **110**, 195002 (2013)]. These studies use a reduced mesoscale model. Model studies reveal that $L \rightarrow H$ transition can be triggered by particle injection into a subcritical state (i.e., $P < P_{\text{Thresh}}$). Particle injection changes edge mean flow shear via changes of density and temperature gradients. The change of edge mean flow shear is critical to turbulence collapse and the subsequent stimulated transition. For low ambient heating, strong injection is predicted to trigger a transient turbulence collapse. Repetitive injection at a period less than the lifetime of the collapsed state can thus maintain the turbulence collapse and so sustain a driven H-mode-like state. The total number of particles required to induce a transition by either injection or gas puffing is estimated. Results indicate that the total number of injected particles required is much smaller than that required for a transition by gas puffing. We thus show that internal injection is more efficient than gas puffing of comparable strength. We also observe that zonal flows do not play a critical role in stimulated transitions. For spontaneous transitions, the spike of the Reynolds work of turbulence on the zonal flow precedes the spike in the mean electric field shear. In contrast, we show that the two are coincident for stimulated transitions, suggesting that there is no causal link between zonal and mean flows for stimulated transitions. © 2013 AIP Publishing LLC. [<http://dx.doi.org/10.1063/1.4818429>]

I. INTRODUCTION

Bifurcations between different system states are ubiquitous in the physics of nonlinear systems. Examples include, but are not limited to, the transition from overturning cells to global circulation in Rayleigh-Bénard convection,¹ first and second order phase transition fronts,^{2,3} nonlinear waves in excitable media,⁴ etc. The class of state bifurcations includes transport bifurcations in confined plasmas, in which the system transitions from a turbulent state of strong anomalous transport to a regime of good confinement. A prime example of such a transition is the well known $L \rightarrow H$ transition.⁵ The H-mode has now become “standard operating procedure,” for tokamak plasmas with good confinement.⁶ Thus, it is the regime anticipated for ITER operation and is thought to be critical to ignition and burning plasma operation. The low(L) \rightarrow high(H) transition requires sufficient heating, fueling, and torque so as to trigger the formation of an edge transport barrier, which is effectively a thermal insulation layer supported by a strong sheared $E \times B$ flow.⁷ The sheared flow is thought to be self-organized by a multi-state evolution involving zonal flow amplification, cyclic oscillations, and eventual “locking in” of a stage of suppressed turbulence by strong diamagnetic $E \times B$ shear.^{8–12} The $L \rightarrow H$ transition has a well defined separatrix heat flux threshold for which the empirical trends have been extensively studied.^{13,14}

The critical role of the H-mode in ignition of a burning plasma has motivated an extensive research effort aimed at achieving control of the $L \rightarrow H$ transition and the associated $H \rightarrow L$ back transition and hysteresis.¹⁵ As a first step toward

control, considerable effort has been expended at understanding (qualitatively and quantitatively) the sequence of zonal and mean flow evolution which occurs during the $L \rightarrow H$ transition.^{12,16} Results indicate that above a certain threshold, Reynolds work of the turbulence on the zonal flow depletes the turbulence energy to the point of collapse. Transport is thus drastically reduced. As a consequence, heating and fueling drive a rapid increase in ∇p_i , generating strong diamagnetic $E \times B$ shear which signals the onset of the H-phase. The physics of this multi-step process ultimately sets the $L \rightarrow H$ threshold. A quantitative model of the threshold power scaling is developing but is not yet complete.^{12,14,17}

A central issue in H-mode physics is to achieve *control*, not only understanding. Control of the $L \rightarrow H$ transition and the $H \rightarrow L$ back transition is desirable, on account of the tight margin for the ITER power threshold and the uncertainty in hysteresis for ITER. Beyond simple performance, however, the capacity to achieve control of the $L \rightarrow H$ bifurcation is the acid test of understanding. Progress from understanding to *control* has been limited. Work in control focused mainly on fueling by transport, i.e., strong-pulsed gas puffing or by pellet injection or super-sonic molecular beam injection (SMBI) as means to improve on standard gas fueling by more effectively optimizing (i.e., increasing) the near edge electric field shear $\langle V_E \rangle'$. Experimental results^{18–21} indicate that

- (i) intense puffing and pellet injection can trigger transitions, sometimes at substantially sub-critical powers.
- (ii) the key element in these fueling-induced transitions seems to be a rapid change in the edge electric field

shear, which is induced by injection. In particular, injection methods or procedures which do not significantly change edge $\langle V_E \rangle'$ seemingly do not induce transitions. Often, the in-practice difference between these approaches which succeed and those which do not is quite subtle.

Moreover, results are rather limited and are not well diagnosed. Results on enhanced hysteresis and back transition control are even more limited. However, the anticipated operation of ITER close to the threshold power has stimulated renewed interest in control of the H-mode.

The recent concern with edge localized model (ELM) mitigation has also motivated a surge in progress in improved injection methods, especially the technologies of small pellets and SMBI, and in understanding the effects of these on edge profiles.^{22,23} Thus, it seems natural to re-visit the physics and dynamics of external transition control, as well. To this end, we have extended our five-field, two predator-one prey model of the L \rightarrow H transition¹² to incorporate a particle source related to internal fueling and the associated cooling process enforced by pressure balance.²⁴ Studies of injection at subcritical powers then reveal

- i) sub-critical transitions can indeed occur.
- ii) the crucial element for a subcritical transition appears to be how the injection influences the edge $\langle V_E \rangle'$, in accord with experimental results. In particular, edge $|V_E|$ must increase sufficiently, for a transition to occur.
- iii) zonal flows do *not* play a key role in such fueling-induced transitions, in contrast to their vital contribution to spontaneous transitions. In particular, there is no identifiable zonal flow precursor to stimulated transitions.
- iv) below a certain power, subcritical injection can induce a *transient* turbulence collapse which later relaxes back to L-mode. The improved confinement state cannot be sustained.
- v) however, repetitive injection *can* sustain subcritical improved H-mode states, thus constituting a kind of “stimulated H-mode.” The duration of such stimulated H-modes can be quite long, even for substantially subcritical powers.
- vi) the variety of stimulated states in the space of SMBI strength, $dQ = (Q_{\text{crit}} - Q)/Q_{\text{crit}}$, x_{dep} , etc., is quite rich. Sensitivities to deposition location and spread are observed, as well.

Moreover, understanding such stimulated transitions is an especially stressing challenge to this, or any, L \rightarrow H model. Any viable model must successfully address both spontaneous and stimulated transitions.

The remainder of this paper is organized as follows. In Sec. II, we introduce our reduced mesoscale model with the additional effects of fueling by SMBI and gas puffing. In Sec. III, we examine several cases of particle injection and its effect on the L \rightarrow H transition. We also quantitatively compare the efficiency of gas puffing to that of SMBI by estimating the total number of particle injected. In Sec. IV,

we compare the role of zonal flows in spontaneous and stimulated transitions. In particular, we show that while a precursor of turbulent Reynolds work on the zonal flow *leads* a spontaneous transition, it occurs *simultaneously* with the growth of mean $\langle V_E \rangle'$ for a stimulated transition. In Sec. V, we summarize this paper and remark open questions and suggestion for future experiments.

II. MODEL

We have previously presented a 5-field reduced meso-scale (envelope) model which evolves turbulence intensity (I), mean square zonal flow shear ($E_0 = V_{ZF}^2$), ion pressure (p) and density (n) profiles, and mean poloidal mass flow ($\langle v_\theta \rangle$) in radius r and time, all in cylindrical geometry. The details of the model are given in Ref. 12. The model equations are

$$\partial_t I = I(\gamma_L - \Delta\omega I - \alpha_0 E_0 - \alpha_V E_V) + \chi_N \partial_r (I \partial_r I), \quad (1)$$

$$\partial_t E_0 = [\alpha_0 I / (1 + \zeta_0 E_V) - \gamma_{\text{damp}}] E_0, \quad (2)$$

$$\begin{aligned} \partial_t p + (1/r) \partial_r [-r(\chi_{i,\text{neo}} + \chi_{i,\text{turb}}) \partial_r p] \\ = Q_a \exp(-r^2/2L_{\text{h,dep}}^2) + \delta\Gamma_{p,\text{SMBI}}, \end{aligned} \quad (3)$$

$$\begin{aligned} \partial_t n + (1/r) \partial_r [-r[(D_{\text{ped}} + D_{\text{turb}}) \partial_r n + V_n n]] \\ = \Gamma_a \frac{a-r+d_a}{L_{\text{dep}}^2} \exp\left[-\frac{(a-r+d_a)^2}{2L_{\text{dep}}^2}\right] \\ + \delta\Gamma_{n,\text{SMBI}} + \delta\Gamma_{n,\text{gaspuff}}, \end{aligned} \quad (4)$$

$$\frac{\partial \langle v_\theta \rangle}{\partial t} = -\alpha_5 \frac{\gamma_L}{\omega_*} c_s^2 \frac{\partial I}{\partial x} - \mu_0^{(\text{neo})} \nu_{ii} q^2 R^2 \left(\langle v_\theta \rangle + 1.17 c_s \frac{\rho_i}{L_T} \right), \quad (5)$$

$$\langle V_E \rangle' = \frac{1}{eB} \left[-\frac{n'p'}{n^2} + \frac{p''}{n} \right] - a \langle v_\theta \rangle'. \quad (6)$$

Here, the essential framework of the model is outlined. Equations (1) and (2) represent a one prey (turbulence intensity)–two predator (zonal flow and mean flow) model, motivated by Ref. 25. The model includes turbulence spreading due to nonlinear scattering. The mean flow shear $E_V = \langle V_E \rangle'^2$ modulates Reynolds drive in the zonal flow evolution. This inhibition is characterized by the factor $\zeta_0 E_V$ in the denominator of Eq. (2). Equations (1) and (2) are the evolutions of mesoscale envelopes. The typical scale size of I and E_0 , $\sim \Delta_{\text{meso}}$, must be satisfied with $l_{\text{micro}} < \Delta_{\text{meso}}$, where $l_{\text{micro}} \sim \rho_i$ ($\sim 0.01a$) is the micro scale size characterized by the ion Larmor radius. To enforce the scale separation between micro and mesoscales, we apply a digital filter to effectively dissipate the short wavelength structure $\Delta_{\text{meso}} < \rho_i$ and to maintain the long wavelength radial structure $\Delta_{\text{meso}} > \rho_i$. Equations (3) and (4) describe heat and particle transport evolution. The diffusion terms consists of the turbulent $\chi_{i,\text{turb}}$, D_{turb} and neoclassical (pedestal) transport $\chi_{i,\text{neo}}$, D_{ped} . Here, the turbulent transport is

proportional to the turbulence intensity, $\chi_{i,\text{turb}} = D_{\text{turb}} \propto I$, while the neoclassical transport is independent of turbulence. We include a particle pinch in the density evolution equation. The pinch velocity consists of turbulent equipartition pinch (TEP) and thermoelectric contributions and can cause density profile peaking. We do not include a heat pinch in the pressure evolution, because the heat source is applied in the core, and we are not concerned with global temperature profile structure. In Eq. (5), we describe the evolution of poloidal mass flow. The poloidal mass flow is both driven by turbulent stress and neoclassical effects. Radial force balance—Eq. (6)—is used to couple the mean $E \times B$ flow and profile (pressure and density) gradients. The radial force balance equation includes pressure curvature, i.e., the second derivative of the pressure profile and poloidal momentum evolution. Note that we here neglect toroidal momentum evolution, for simplicity. Future extensions of the model will evolve toroidal velocity. We impose free edge boundary condition on I , E_0 , and $\langle v_\theta \rangle$, by neglecting scrape-off-layer (SOL) edge coupling. p and n are set to be fixed on the edge boundary. We also neglect any MHD activity, such as ELMs.

The set of parameters we used in this simulation is $\rho_i = 0.01a$, $\epsilon_t = a/R = 0.25$, $L_{\text{h,dep}}/a = 0.15$, $L_{\text{dep}}/a = 0.10$, $d_a/a = 0$, $\tau_c = 10a/c_s$, $\alpha_t = 1.0(a/c_s)^2$, $\gamma_{L0} = \Delta\omega 10^{-2}(c_s/R)$, $\alpha_0 = 10^2 \sqrt{\rho_*}(c_s/a)$, $\alpha_V = 10^{-1} \sqrt{\rho_*}(c_s/a)$, $\zeta_0 = 5.0 \times 10^3 (a/c_s)^2$, $(R/L_T)_{\text{crit}} = 3.7$, $\gamma_{\text{damp}} = 2.0\nu_{ii}/R(c_s/a)$, $\chi_N = 0.5\rho_* (a/c_s)^2$, $\mu_{00} = 1.0a^{-2}$, $\alpha_5 = 5.0 \times 10^3$, and $V_{n0} = 1.0$. Radial space and time scales are normalized by the minor radius a and the characteristic time of drift wave $\omega_*^{-1} = (a/c_s)$, respectively. The density and pressure are normalized by the reference density, $n_0 = 10^{20}[\text{m}^{-3}]$, and pressure, $p_0 = T_{i0}n_0 = 1[\text{keV}] \times 10^{20}[\text{m}^{-3}]$, respectively.

To address the effect of pellets, SMBI, etc., we include additional fueling $\delta\Gamma_{n,\text{SMBI}}$ and $\delta\Gamma_{p,\text{SMBI}}$ in the density and pressure equation. The density equation modification by pellet injection or SMBI is

$$\delta\Gamma_{n,\text{SMBI}} = \frac{I_{\text{SMBI}}(n_{\text{ref}})}{\tau_{\text{SMBI}}} \sum_i [H(t - t_i) - H(t - t_i - \tau_{\text{SMBI}})] \times f\left(\frac{a - x_{\text{dep}}}{\Delta x}\right). \quad (7)$$

Here, the important parameters characterizing particle injection are I_{SMBI} : the strength of particle injection proportional to the total number of particle injection, τ_{SMBI} : the duration of particle injection, x_{dep} : the deposition depth, and Δx : the width of deposition (all are illustrated in Fig. 1). $H(t)$ is Heaviside function. $f(x) \equiv \exp(-x^2/2)$ is a Gaussian representing the shape of deposition. $n_{\text{ref}} = 0.11n_0$ is a coefficient, referring to the density at $r/a = 0.975$ (see Fig. 2(d)). Reference values for these factors are $x_{\text{dep}} = 0.975a$, $\Delta x = 0.02a$, $\tau_{\text{SMBI}} = 250(a/c_s)$, $I_{\text{SMBI}} = 10 - 50$. We select these parameters to be consistent with realistic values from SMBI experiments.²³

For the pressure perturbation, we note $\delta\Gamma_{p,\text{SMBI}} \sim 0$ on times long compared to the acoustic time scale $\tau > R/c_s$, due to pressure balance. We assume that the sound waves will relax the SMBI-induced pressure perturbation quickly on the time scale R/c_s . Note also that the identity $p = nT$ implies cooling due to particle injection, i.e.,

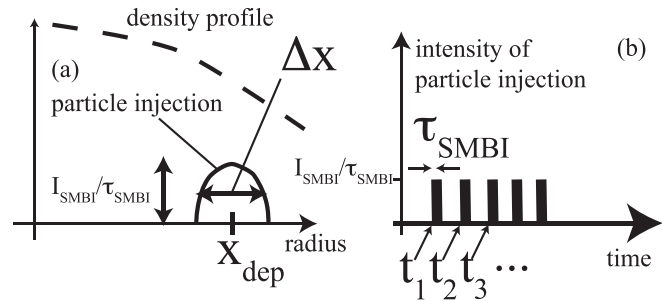


FIG. 1. Illustrations of particle injection (a) showing the deposition structure, with the location of deposition x_{dep} , the width of deposition Δx , and the intensity of particle injection I_{SMBI} . (b) The time evolution of particle injection. The duration of particle injection is τ_{SMBI} . Reproduced with permission from Miki *et al.*, Phys. Rev. Lett. **110**, 195002 (2013). Copyright 2013 American Physical Society.

$$\delta\Gamma_{T,\text{SMBI}} = -\frac{T_{\text{ref}}}{n_{\text{ref}}} \delta\Gamma_{n,\text{SMBI}}. \quad (8)$$

Thus, the temperature decreases due to particle injection, on account of $\delta p \sim 0$.

We also model time dependent gas puffing from an edge source by adding the new term $\delta\Gamma_{n,\text{gaspuff}}$ to the density equation, i.e.,

$$\delta\Gamma_{n,\text{gaspuff}} = \delta\Gamma_a \frac{a - r + d_a}{L_{\text{dep}}^2} \exp\left[-\frac{(a - r + d_a)^2}{2L_{\text{dep}}^2}\right] \times \sum_i [H(t - t_i) - H(t - t_i - \tau_{\text{gaspuff}})]. \quad (9)$$

For simplicity, we assume that gas puffing uniformly modulates fueling effects, thus neglecting source poloidal and toroidal asymmetry. The fueling source, $\Gamma_a + \delta\Gamma_a$, replaces Γ_a in the first term of r.h.s. of Eq. (4), during the time τ_{gaspuff} . The duration of gas puffing is assumed to be longer than that of particle injection. We choose $\tau_{\text{SMBI}} = 250a/c_s \sim 1$ ms and $\tau_{\text{gaspuff}} = 3000a/c_s \sim 10$ ms, to be consistent with experiments.^{18,23}

Keep in mind that there are many limitations of this reduced model. Regarding injection, there is no treatment of ablation and the ionization process. Injection is modeled as instantaneous, so the time delay related to ionization, etc., is not accurately represented. Thus, we may not accurately model deep particle injection. We do not consider toroidal and poloidal source asymmetry. Also, the model does not evolve toroidal rotation V_ϕ , and so does not account for possible benefits from reduction in rotation due to injection. In addition, we should independently evolve ion and electron temperatures, with separate ion and electron heating, to reproduce the low $P_{\text{Th}}(n)$ behavior.^{14,26} To make that simulation meaningful, we also need to generalize turbulence model to include trapped electron modes (TEMs) as well as ion temperature gradient (ITG) turbulence. In particular, fueling may result in a steepen density gradient, in which TEM may be dominant. In future work, we will include edge electron temperature $T_e(r/a = 1)$ effects on SOL heat transport¹⁷ and treat lower-single-null (LSN) vs upper-single-null (USN) asymmetry.²⁷

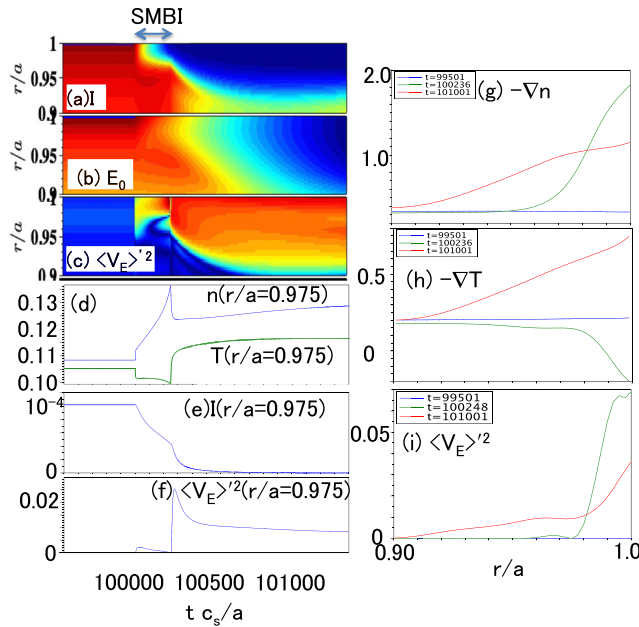


FIG. 2. Results for model calculation, case 1: ($t_1 = 10^5 a/c_s$, $I_{\text{SMBI}} = 30$, $\tau_{\text{SMBI}} = 250a/c_s$, $x_{\text{dep}}/a = 0.975$, $\Delta x/a = 0.02$, $dQ = 0.5$, particle injection occurs during $t = 100\,000 - 100\,250a/c_s$). (a)–(c) Spatio-temporal evolution of turbulence intensity I , zonal flow energy E_0 , and mean flow energy $\langle V_E \rangle'^2$, respectively. Evolution of (d) density and temperature, (e) turbulence intensity I , and (f) mean flow shear $\langle V_E \rangle'^2$, at $r/a = 0.975$, respectively. (g) and (h) Profiles of $-\nabla n$ and $-\nabla T$ at $t = 99\,501a/c_s$ (blue, before injection), $t = 100\,236a/c_s$ (green, during injection), and $t = 101\,001a/c_s$ (red, after injection), respectively. (i) Profile of $\langle V_E \rangle'^2$, before, during, and after injection. Reproduced with permission from Miki *et al.*, Phys. Rev. Lett. **110**, 195002 (2013). Copyright 2013 American Physical Society.

III. MODEL STUDIES

In this section, we examine several paradigmatic cases of particle injection and its effect on the L \rightarrow H transition. First, we discuss a case where injection triggers the L \rightarrow H transition (case 1). Then, we present a different case for which deeper injection does *not* trigger L \rightarrow H transition but rather excites a damped relaxation oscillation (case 2). We discuss the comparison of these two cases. Next, we discuss net “gain” from SMBI (i.e., internal injection), to answer the questions: though both SMBI and gas puff perturb profiles, how do we quantify the difference between the two? Is it clear that for equal number of injection of particles, SMBI is more effective at inducing transition than strong gas puffing is? By estimating the total number of particles injected, we *quantitatively* compare gas puffing to SMBI and assess their effects on the transition. Results unambiguously show that for equal number of injected particles, SMBI is more effective at inducing transition than strong gas puffing is, on account of its better leverage in edge profiles. Next, we show a case where injection into a subcritical state triggers a transient turbulence collapse (case 3). We then examine sequential injection into the subcritical state, thereby maintaining the state of turbulence collapse (case 4). Finally, we map out the trends in the parameter space of injection intensity I_{SMBI} and the degree of deviation from the critical heat flux $dQ = (Q_{\text{crit}} - Q_a)/Q_{\text{crit}}$. Here, Q_{crit} is the critical edge heat flux threshold for which the L \rightarrow H transition occurs

spontaneously. We also discuss the sensitivity of the transition to deposition location.

A. Edge $\langle V_E \rangle'$ structure

Case 1 (Fig. 2) shows that particle injection triggers a subcritical L \rightarrow H transition. We set a moderate intensity of injection ($I_{\text{SMBI}} = 30$), with shallow deposition ($x_{\text{dep}} = 0.975a$). These parameters are consistent with those from SMBI experiments. Heating is subcritical ($dQ = 0.5$), so the system is in L-mode and no limit-cycle oscillation (LCO) appears. As seen in Figs. 2(a)–2(c), the L \rightarrow H transition is triggered by the immediate collapse of edge turbulence upon injection. Then the turbulence collapse expands inwards. The excitation of mean flow shear follows the turbulence collapse after injection. Then, strongly excited mean flow shear expands inward and locks in H-mode. Due to particle injection, density increases, so $\Delta n/n \sim 22\%$, and temperature decreases $\Delta T/T \sim -5.7\%$, as seen in Fig. 2(d). As seen in Figs. 2(g) and 2(h), the density gradient peaks at the edge during injection, and the temperature profile flattens locally at the edge. After injection, both the temperature and density gradients remain peaked at the edge. Turbulence is quickly quenched following injection, as seen in Fig. 2(e). After injection, a single rapid burst in $\langle V_E \rangle'^2$ (in Fig. 2(f)) is followed by its relaxation to the H-phase value with enhanced edge $\langle V_E \rangle'$, as seen in Fig. 2(i). After injection, rapidly growing $\langle V_E \rangle'$ locks in the transition, so a transport barrier is formed at the edge. Fueling induces transitions by driving the edge $\langle V_E \rangle'$ sufficiently to exceed a threshold for quenching turbulence.

Case 2 (Fig. 3) shows that deeper injection triggers a *damped* oscillation. It is important to note this is *not* an LCO. We set the same deposition parameters as for case 1, but with a slightly deeper deposition location of $x_{\text{dep}} = 0.95a$, instead of $x_{\text{dep}} = 0.975a$. As seen in Figs. 3(a)–3(c), edge turbulence is not completely quenched after injection but recovers during a damped oscillation of turbulence, zonal flow, and mean flow. A key difference from case 1 is that the edge $\langle V_E \rangle'$ is not enhanced, as shown in Fig. 3(d).

Note that the observed oscillation here is *not* an I-phase. I-phase occurs when a transient fixed point is destabilized by mean flow shear, so that a limit-cycle oscillation is established as a stationary state. This state of damped oscillation is one where the transient fixed point is not fully destabilized by mean flow shear. This oscillatory state decays to L-mode.

The lesson learned here is that *edge* mean shear $\langle V_E \rangle'$ is critical to turbulence collapse and the L \rightarrow H transition. Despite comparable injection scenarios, the case with stronger $\langle V_E \rangle'$ at the edge produces a transition, while for the case with weak $\langle V_E \rangle'$ at the edge, the transition does *not* occur. This finding is consistent with the experiential results from Tuman-3.¹⁸ Without L \rightarrow H transition, damped oscillation occurs. Also, observe that in those transitions, the zonal flow appears to play no significant role. We will discuss the issue of zonal flow physics in the transition further in Sec. IV.

B. Quantitative comparison of SMBI and gas puffing

In this subsection, we address the oft-asked question concerning the relative merits of gas puffing and SMBI. *In*

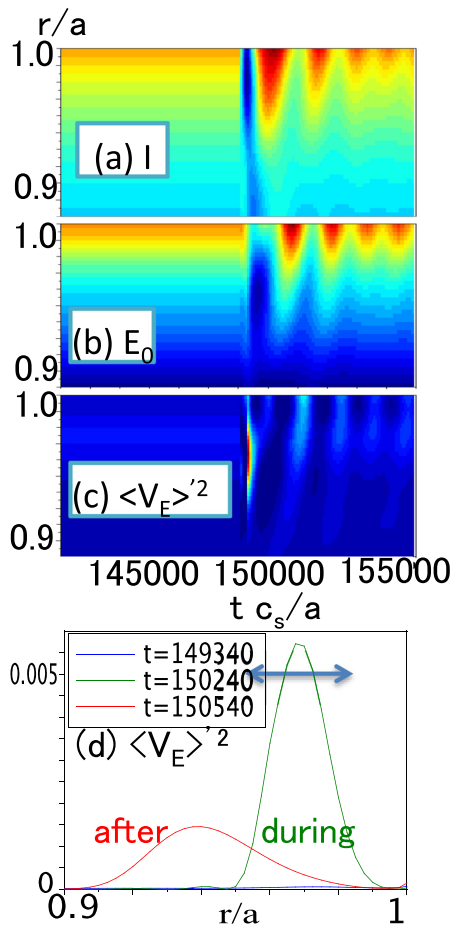


FIG. 3. Results of model calculation, case 2 ($t_1 = 10^5 a/c_s$, $I_{\text{SMBI}} = 30$, $\tau_{\text{SMBI}} = 250 a/c_s$, $x_{\text{dep}}/a = 0.95$, $\Delta x/a = 0.02$, $dQ = 0.5$): (a)–(c) Spatio-temporal evolution of turbulence intensity, zonal flow, and mean flow, respectively, and (d) profile of $\langle V_E \rangle'^2$ during ($t = 150240 a/c_s$) and after ($t = 150540 a/c_s$) injection. During the injection, the peak of the mean flow is off the edge.

particular, we aim to elucidate precisely how much better SMBI is for triggering transitions than gas puffing is. We here introduce quantitative comparisons of the total number of particles necessary to trigger $L \rightarrow H$ transition by SMBI with that using gas puffing. This comparison is a basic measure of the relative efficiency of the two fueling methods. We first show an $L \rightarrow H$ transition triggered by simple gas puffing in Fig. 4. In the density equation, Eq. (4), we have two particle sources, $\delta\Gamma_{\text{SMBI}}$ and $\delta\Gamma_{\text{gas puff}}$. Now, we use $\delta\Gamma_{\text{gas puff}}$ for gas puffing. As in the case of transition by particle injection (Fig. 2), turbulence collapses and mean flow increases and expands after a period of gas puffing of duration $\tau_{\text{gas puff}} = 3000 a/c_s$. Thus, we see gas puffing alone can trigger the $L \rightarrow H$ transition! By further simulations with various ratios of $\delta\Gamma_a/\Gamma_a$, we estimate the critical intensity of gas puffing for triggering transition to be $3.5 < \delta\Gamma_a/\Gamma_a < 3.6$.

Now, we estimate the total number of particles introduced by gas puffing. Integrating $\delta\Gamma_{n, \text{gas puff}}$ in Eqs. (4) and (9) in space and time, the total number of particles is

$$\Delta N_{\text{gas puff}} = \iint dV dt \delta\Gamma_{n, \text{gas puff}} \sim (2\pi)^2 a R \tau_{\text{gas puff}} \delta\Gamma_a. \quad (10)$$

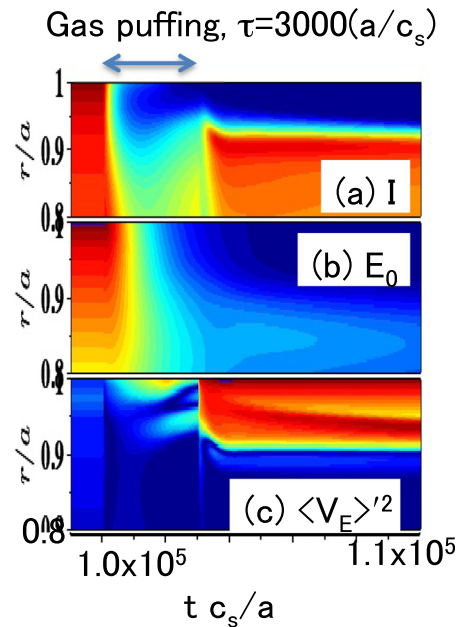


FIG. 4. Spatio-temporal evolution of (a) turbulence, (b) zonal flow, (c) mean flow shear $\langle V_E \rangle'^2$ in the case of gas puffing ($\delta\Gamma_a/\Gamma_a = 3.6$).

Substituting $\Gamma_a = 10^{-4} (n_0 c_s)$, $\delta\Gamma_a/\Gamma_a = 3.6$, $\tau_{\text{gas puff}} = 3000 a/c_s$, and $R/a = 4$, we obtain the total number of particles introduced by gas puffing to be $\Delta N_{\text{gas puff}} = 1.71 \times 10^2 (a^3 n_0)$. Note that $(a^3 n_0)$ is a normalized unit of the number of particles. We now compare the number of particles added by gas puffing to that added by particle injection, by examining the case of particle injection with edge deposition, $x_{\text{dep}} = a$, and find the critical intensity of injection to lie in the interval $25 < I_{\text{SMBI}} < 30$. Integrating $\delta\Gamma_{n, \text{SMBI}}$ in Eqs. (4) and (7) in space and time, the total number of particles injected is seen to be

$$\begin{aligned} \Delta N_{\text{SMBI}} &= \iint dt dV \delta\Gamma_{n, \text{SMBI}} = \int dV \int dt \frac{I_{\text{SMBI}}(n_{\text{ref}})}{\tau_{\text{SMBI}}} \\ &\quad \times \sum_i [H(t - t_i) - H(t - t_i - \tau_{\text{SMBI}})] \\ &\quad \times \exp\left(-\frac{(r - x_{\text{dep}})^2}{2\Delta x^2}\right) \\ &\simeq (2\pi)^2 a R \sqrt{2\pi} f_{x_{\text{dep}}} \Delta x I_{\text{SMBI}}(n_{\text{ref}}), \end{aligned} \quad (11)$$

where

$$f_{x_{\text{dep}}} = \begin{cases} \sim 1 & (\text{for } x_{\text{dep}} = 0.975a) \\ 0.5 & (\text{for } x_{\text{dep}} = a). \end{cases} \quad (12)$$

Substituting $\Delta x = 0.02a$ and $I_{\text{SMBI}} = 30$, we obtain $\Delta N_{\text{SMBI}} = 13(a^3 n_0)$.

The comparison of $\Delta N_{\text{gas puff}}$ and ΔN_{SMBI} indicates that *particle injection*—a short pulse of internal (but shallow) particle deposition—*clearly triggers the transition with much fewer particles, than gas puffing does. The large difference between the total number of particles indicates that the injection causes a change in edge profiles and $\langle V_E \rangle'$, which is essential for the transition. Short, intense particle pulsation*

can more easily induce profile and $\langle V_E \rangle'$ changes with a smaller total number of particles than gas puffing can.

We also examined the case of particle injection with the same duration as for gas puffing, i.e., $\tau_{\text{SMBI}} = 3000a/c_s$. We estimate the critical intensity of SMBI to be $350 < I_{\text{SMBI}} < 360$. Substituting $I_{\text{SMBI}} = 360$, we obtain $\Delta N_{\text{SMBI}} = 1.61 \times 10^2 (a^3 n_0)$. This is similar to the number of particles added by gas puffing $\Delta N_{\text{gas puff}} = 1.71 \times 10^2 (a^3 n_0)$!

The lesson learned here is that in terms of particle numbers, gas puffing is semi-quantitatively equivalent to particle injection, for fixed duration of injection. However, profile change is necessary to trigger the transition rather than dependence on only the number of particles injected. Intense and rapid particle injection is beneficial for transition, as opposed to weak and slow gas puffing, since injection promotes edge profile and $\langle V_E \rangle'$ changes which favor the transition.

C. Effective hysteresis

Case 3 (Fig. 5) shows that injection into a subcritical state triggers *transient* turbulence collapse. Here, we use a lower ambient heating power, $dQ = 0.7$, than in case 1. In Fig. 5, after injection, the turbulence collapses, recovers, and then returns to L-mode. During the collapse, $\langle V_E \rangle'$ exhibits a transient burst. Once the system enters the transient H-mode, weak heating does not sustain a mean flow shear sufficient to quench the turbulence. The turbulence then advances or spreads from the core into the quiescent edge region. This process resembles that observed in the H \rightarrow L back transition.^{15,28} As seen in Fig. 5(b), the zonal flow appears to be dragged along by the turbulence, since turbulence drives zonal flow.

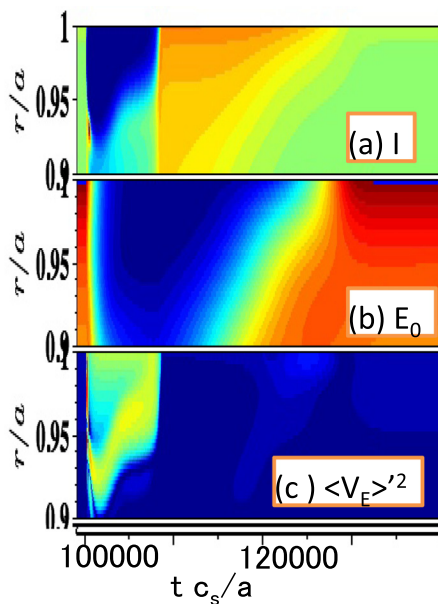


FIG. 5. Results of model calculation, case 3: ($t_1 = 10^5 a/c_s$, $I_{\text{SMBI}} = 50$, $\tau_{\text{SMBI}} = 250a/c_s$, $x_{\text{dep}}/a = 0.975$, $\Delta x/a = 0.02$, $dQ = 0.7$, particle injection is induced during $t = 100\,000 - 100\,250a/c_s$). (a)-(c) Spatio-temporal evolution of turbulence intensity, zonal flow, and excitation of mean flow) is transiently excited but turns back to L-mode at $t \sim 1.1 \times 10^5 a/c_s$.

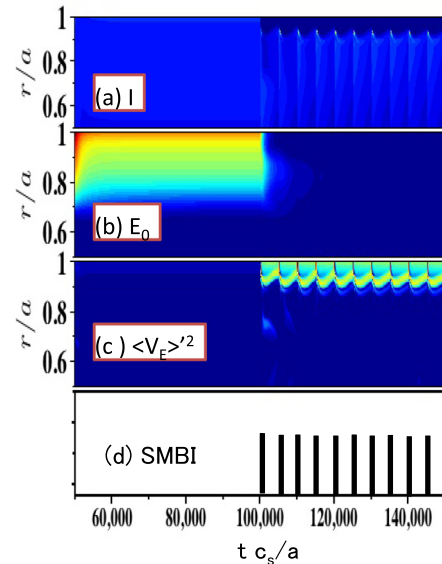


FIG. 6. Results of model calculation, case 4: ($t_i = 100\,000 + 5000ia/c_s$ ($i = 0, 1, \dots$) (i.e., sequential shots), $I_{\text{SMBI}} = 50$, $\tau_{\text{SMBI}} = 250a/c_s$, $x_{\text{dep}}/a = 0.975$, $\Delta x/a = 0.02$, $dQ = 0.7$). (a)-(c) spatio-temporal evolution of turbulence intensity, zonal flow, and mean flow, respectively. Repetitive, sequential particle injection sustains edge $\langle V_E \rangle'$, thus H-mode maintains. Reproduced with permission from Miki et al., Phys. Rev. Lett. 110, 195002 (2013). Copyright 2013 American Physical Society.

Case 4 (Fig. 6), however, shows that *sequential, repetitive injection into a subcritical state can sustain the turbulence collapse*. Here, we inject particles every $5000a/c_s$. This sustainment of turbulence collapse may be thought of a “driven H-mode.” Through the repetitive, sequential injection, edge $\langle V_E \rangle'$ exhibits continuous enhancement. By subsequent injection before the system returns to the L-mode, the system can maintain the stimulated H-mode-like state. We find that stronger I_{SMBI} results in a longer transient H-mode. Thus, the important factors which determine the “driven H-mode” state are I_{SMBI} , dQ , and the frequency of sequential particle injection f_{SMBI} . Further study of this transient imposed state will be pursued in the future.

The lesson learned is that injection can trigger transient turbulent collapse in a subcritical regime. Repetitive, sequential injection can sustain subcritical turbulence collapse, i.e., a “stimulated” H-mode. We speculate that sequential injection can enhance effective hysteresis, facilitating control of the H \rightarrow L back transition. Indeed, sequential SMBI sometimes delays the H \rightarrow L back transition in HL-2A.²¹

D. Characteristics of stimulated transitions

It is natural to ask what are the characteristics of these stimulated subcritical transitions? One clue comes from the study of heat flux variability.²⁶ There we noted that intrinsic heat flux noise, i.e., heat avalanches, can trigger subcritical transitions. Many anecdotes exist describing sudden transitions in stationary, somewhat subcritical states. The transition dynamics in these cases is likely non-deterministic and unpredictable, due to noisy avalanching driven by micro turbulence. As a consequence, the edge is continuously bombarded by an ensemble of micro heat pulses.²⁹ We have investigated transition dynamics by exploring the transition

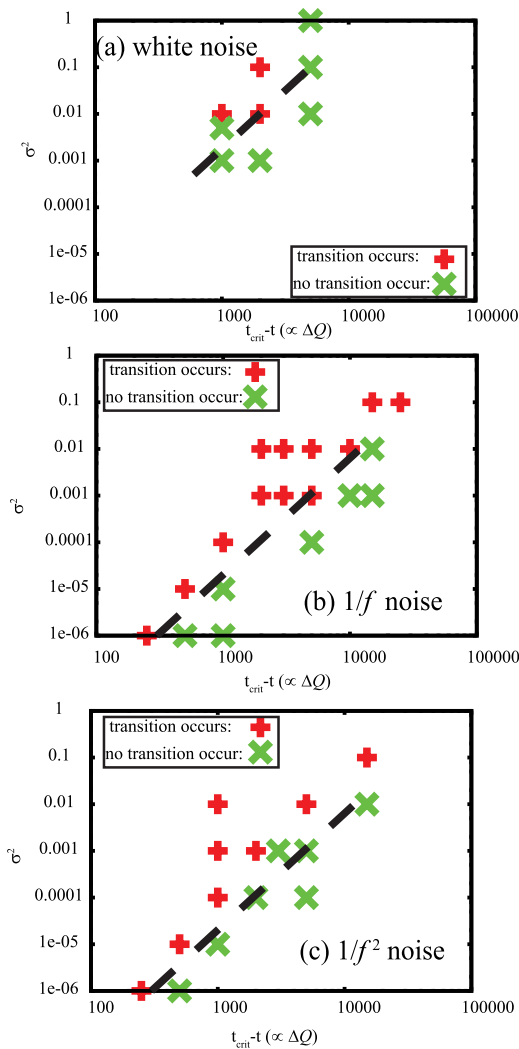


FIG. 7. Scan of transition occurrence in space of noise intensity (σ^2) vs margin of subcriticality (dQ), with different noise colors: (a) white, (b) $1/f$, and (c) $1/f^2$. Reproduced with permission from Miki *et al.*, Nucl. Fusion **53**, 073044 (2013). Copyright 2013 IOP Publishing.

behavior in the space of heat flux noise intensity $\langle \sigma^2 \rangle = \langle (\tilde{Q} - \langle Q_a \rangle)^2 \rangle / \langle Q_a \rangle$ vs margin of sub-criticality $dQ = (Q_{\text{crit}} - \langle Q_a \rangle) / Q_{\text{crit}}$, taking into account different spectral dependency of noise, i.e., white, $1/f$, and $1/f^2$. Results of model studies have confirmed that sufficient heat flux noise variability can trigger subcritical transition. These are shown in Fig. 7. For lower ambient mean heating (i.e., higher dQ), we need higher noise intensity $\langle \sigma^2 \rangle$ to trigger subcritical transition. The subcritical transitions occur more easily for $1/f$ than for white noise of equal net intensity. This is likely due to longer shearing self-correlation times at low frequency.

Returning to the question of particle injection, Fig. 8(a) shows transition behavior for different values of I_{SMBI} and dQ . We here identify four types of outcomes, i.e., no transition (L-mode to L-mode after injection), L \rightarrow I transition (L-mode to I-phase after injection—here, the I-phase is a steady LCO), on-edge transition (L \rightarrow H transition, where the H-mode is triggered at the edge by an increased edge $\langle V_E \rangle$), and off-edge transition (L \rightarrow H transition where the H-mode is triggered off the edge by strong $\langle V_E \rangle$ away from

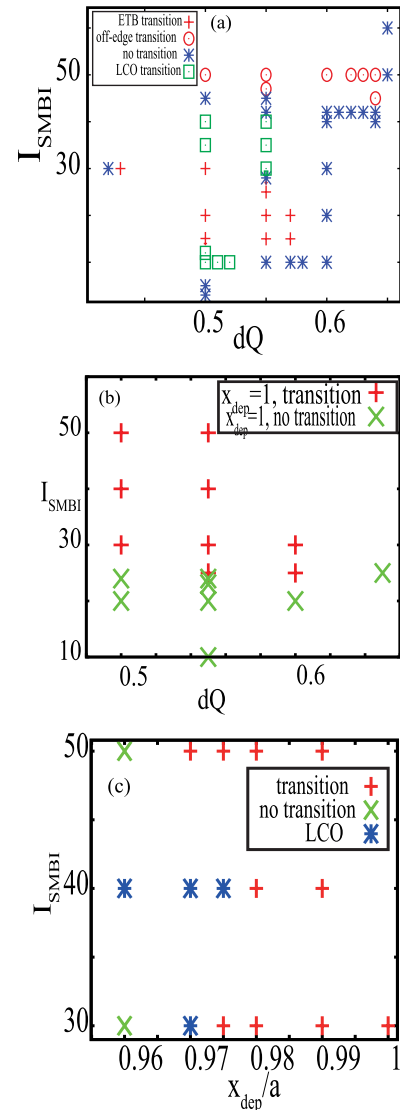


FIG. 8. Graphs of transition occurrence in space of I_{SMBI} vs dQ , for (a) $x_{\text{dep}}/a = 0.975$ and (b) $x_{\text{dep}}/a = 1.0$, with fixed $dQ = 0.5$. (c) Plots of transition occurrence in space of x_{dep} vs I_{SMBI} with fixed $dQ = 0.5$.

the edge). Lower ambient heating (i.e., higher dQ) requires higher I_{SMBI} to trigger a transition. However, for sufficiently low heating, e.g., $dQ = 0.7$, the standard L \rightarrow H transition never occurs. Turbulence can collapse *transiently* though the system ultimately returns to the turbulent L-mode (see case 3 (Fig. 5)). The on-edge transition is one for which the edge $\langle V_E \rangle$ is enhanced rapidly (see case 1 (Fig. 2)). These various transitions are summarized in Table I.

Off-edge transitions are ones for which sufficiently strong particle injection excites strong yV_E' away from the edge, without an initial change of edge $\langle V_E \rangle$. A case of off-edge transition is shown in Fig. 9. There, transition begins off the edge and then the collapse of turbulence spreads both inward and outward, triggering an increase in $\langle V_E \rangle$ at the edge. Off-edge transitions seem to occur when the fueling zone does not overlap the edge. This occurs when $x_{\text{dep}} + \Delta x < a$. Curiously, an L \rightarrow H transition does *not* occur between the values of I_{SMBI} for off-edge and on-edge transitions, i.e., in the range $30 < I_{\text{SMBI}} < 50$ at $dQ = 0.5$, as

TABLE I. Summary of different types of injection-induced transitions, classified by the final states of transition, from L-mode to H-mode, from L-mode to I-phase, and L-mode persists through the transition.

| Transition from/to | Type of transition | Examples | Description |
|--------------------|--------------------|------------------------|--|
| L → H | Off-edge | Fig. 9 | Transition initiates off the edge |
| | On-edge | Fig. 2 (case 1) | Transition initiates on the edge |
| L → I | LCO | N/A | Transitions to a stationary LCO |
| L → L | Damped oscillation | Fig. 3 (case 2) | A damped oscillation returns to L-mode |
| (No transition) | Transient H-mode | Fig. 5 (cases 3 and 4) | H-mode is transiently excited |
| | No transient mode | N/A | w/o transient mode, L-mode recovers |

seen in Fig. 8(a). In this range of I_{SMBI} values, edge $\langle V_E \rangle'$ does not increase sufficiently during injection, and the off-edge peak of $\langle V_E \rangle'$ is not large enough to cause a change in edge $\langle V_E \rangle'$, upon relaxation. Note that this complicated behavior may be an effect of the rather crude model we use. A complete model of injection should include the wake due to the processes of pellet or gas jet penetration, ablation, ionization, etc. Therefore, such off-edge transitions may not be identifiably distinct phenomena. Further work on the injection model is required.

To clarify the findings, we also investigate edge deposition. Note that edge deposition, $x_{\text{dep}} = a$, results in a simpler decomposition of the I_{SMBI} vs dQ domain (see Fig. 8(b)) by eliminating the second class (i.e., “off-edge”) of transition. Figure 8(c) shows transitions mapped in the space of x_{dep} vs I_{SMBI} , with fixed $dQ = 0.5$. We observe that the intermediate LCO region disappears for $x_{\text{SMBI}} \geq 0.98a$.

The lesson learned here is that various—indeed many—types of transitions are possible: LCO and on-edge transitions occur for weaker I_{SMBI} , and off-edge transitions occur for higher I_{SMBI} . For example, with increasing I_{SMBI} and

fixed $dQ = 0.5$, the dynamics evolves from no transition, to LCO, to on-edge transition, back to LCO, to no transition, and finally to off-edge transitions. We observe that zonal flow does not exhibit any peak or burst in the on or off-edge transition cases (Fig. 2(b)).

IV. A ROLE OF ZONAL FLOWS IN SPONTANEOUS AND STIMULATED TRANSITIONS

In this section, we discuss what fundamentally triggers transitions, with special emphasis on zonal flows. It seems that zonal flow does not exhibit any pre-transition peaking or burst in the case of stimulated transition, triggered by injection. As seen in case 1 (Fig. 2(b)), zonal flows seem to damp immediately after transition. There is no evidence of zonal flow burst prior to, or at the transition, but the edge $\langle V_E \rangle'$ indeed seems to be a key to the stimulated transition. However, without any external source or noise, and with increasing heat flux (i.e., a power ramp), the L → H transition *spontaneously* evolves via the mediation of zonal flow, which appears to play a central role. There, the zonal flow acts as “holding pattern” in which to store increasing fluctuation energy without increasing transport, thus allowing the mean flow shear to increase and lock in the transition.¹² In particular, in the spontaneous transition, a peak in the normalized Reynolds work of the turbulence on the zonal flow has been shown to *precede* the transition.¹⁶ Given the contrast between the findings for spontaneous and stimulated transitions, further study and clarification are required.

Based on the predator-prey model, we explore the roles of zonal flow and mean flow in the two kinds of transitions by introducing the following parameters^{12,16}

$$R_T = \frac{\alpha_0 E_0}{\gamma_L - \Delta \omega I}, \quad (13)$$

$$R_H = \frac{\alpha_V E_V}{\gamma_L - \Delta \omega I}. \quad (14)$$

Here, R_T measures the rate of energy transfer from turbulence into zonal flow, normalized by the rate of energy input into the turbulence. When R_T exceeds order unity, the turbulence can collapse, allowing rapid steepening of ∇p . Turbulence collapse occurs due to coupling of fluctuation energy to the zonal flow. R_H is the rate of shearing of the turbulence by the mean flow, normalized by the energy input into the turbulence. When R_H exceeds order unity, turbulence is quenched by mean flow shearing, leading to locking

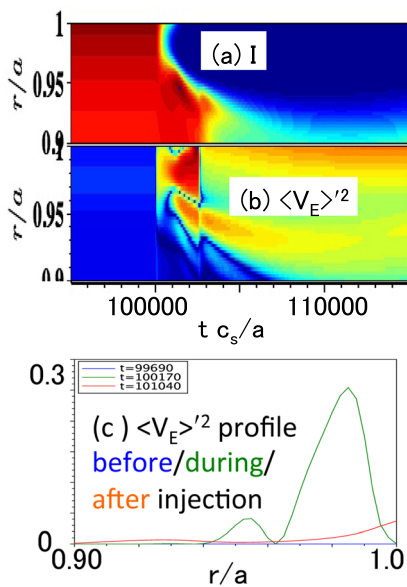


FIG. 9. Results of model calculation, the case of off-edge transition: ($t_1 = 10^5 a/c_s$, $I_{\text{SMBI}} = 50$, $\tau_{\text{SMBI}} = 250 a/c_s$, $x_{\text{dep}}/a = 0.975$, $\Delta x/a = 0.02$, $dQ = 0.5$). (a) and (b) Spatio-temporal evolution of turbulence intensity and mean flow, respectively. (c) Profile of mean flow shear $\langle V_E \rangle'^2$ during (green, peaked off the edge) and after (red, peaked at the edge) the injection. During the transition, the peak of the mean flow shear off-edge and the turbulence collapse starts off edge and then spreads inward and outward.

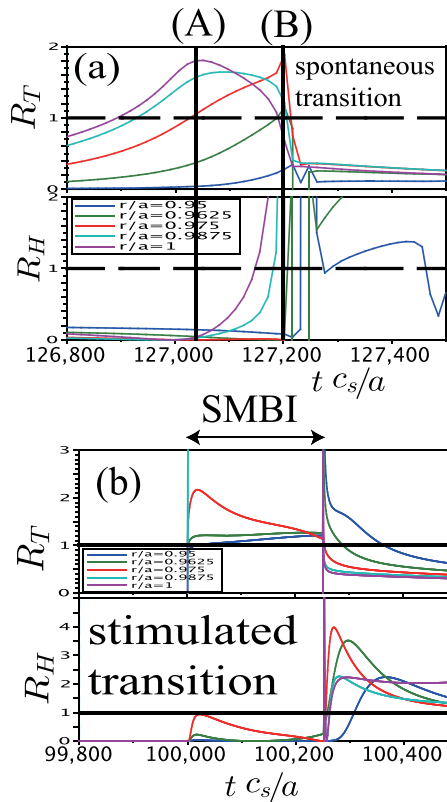


FIG. 10. Temporal evolution of R_T and R_H , at various radial locations $r/a = 0.95, 0.9625, 0.975, 0.9875, 1.0$ for the case of (a) spontaneous, and (b) stimulated L \rightarrow H transitions. Reproduced with permission from Ref. Miki *et al.*, Phys. Rev. Lett. **110**, 195002 (2013). Copyright 2013 American Physical Society.

in of the H-mode. We track R_T and R_H evolution in the spontaneous and stimulated transitions. In particular, the time ordering of the peaks of R_T and R_H reveal a great deal about the roles of zonal and mean flows in the transitions.

Figure 10 contrasts evolution of R_T and R_H for the spontaneous (no particle injection, gradually increasing heat flux) and stimulated (with particle injection, and fixed heat flux) transitions. For the case of the spontaneous transition (Fig. 10(a)), the peak of R_T at $r/a = 1.0$ (at time (A)) clearly *precedes* the peak in R_H at $r/a = 1.0$ (at time (B)). This sequence suggests a causal relation between zonal flow and mean flow at the edge. The edge zonal flow absorbs fluctuation energy without increasing edge transport (zonal flows have $n = 0$), thus subsequently allowing the edge mean flow shear to increase and lock in the transition, as shown by the peak in R_H which *follows* that of R_T . Once the value of R_H peaks at the edge, peaking of values at inner locations follows, suggesting that the transition expands inward. This is consistent with visualizations of the transition evolution.

For the case of the stimulated transition (Fig. 10(b)), the peaks of R_T and R_H *coincide*. This result suggests that the zonal flow coupling is *not* critical for stimulated transitions, due to injection and that there is no causal link between zonal and mean flows in such transitions. We note, then, that the spontaneous and stimulated transitions take fundamentally different routes to achieve transport and profile bifurcation. The spontaneous transition occurs via zonal flow excitation and shearing to reduce turbulence and transport,

and increase ∇p_i . On the other hand, the stimulated transition steepens $\nabla \langle p_i \rangle$ and $\langle V_E \rangle'$ via direct injection effects on edge gradients. Stronger shear in $\langle V_E \rangle'$ immediately quenches turbulence and, with it, zonal flows. Though these routes to transition differ, there is *no fundamental contradiction*.

We note that the models (and its parameters) used to study spontaneous and stimulated transitions are equivalent, apart from the addition of internal fueling effects for the stimulated case. The density profile perturbation, due to particle injection, favorably excites edge $\langle V_E \rangle'$. The edge $\langle V_E \rangle'$ enhancement should be sensitive to boundary conditions. Further studies of stimulated transitions, regarding more general boundary, i.e., effects of SOL-edge interaction,¹⁷ poloidal asymmetry,²⁷ etc., are necessary in the future.

External sources can possibly delay the H \rightarrow L back transition. For sufficiently low ambient heating, strong transient particle injection can cause turbulence collapse, as shown in case 3 (Fig. 5). Moreover, repetitive injection can maintain a state of turbulence collapse, as shown in case 4 (Fig. 6). Making use of repetitive injection can possibly control both the L \rightarrow H and H \rightarrow L transitions and thus enhance hysteresis. Repetitive injection can constitute a knob for controlling the extent of the hysteresis in heat flux Q .

Heat pulses, as well as particle injection, can also induce transitions.³⁰ Indeed, heat pulse induced transitions have been observed since the earliest days of H-mode research.²⁹ On HL-2A, they observed that quasi-periodic sawtooth heat pulses bombarding the edge induces L \rightarrow I \rightarrow L transition evolution. Model studies reveal that L \rightarrow I transition occurs for higher ambient heating, while for lower ambient heating, the oscillation excited gradually decays to L-mode. Just as repetitive particle injection can sustain a driven H-mode, one naturally wonders if repetitive sawtooth pulses can also sustain I-phase or H-mode? For a single heat pulse, damped oscillations occur when edge mean flow is not sufficiently excited to destabilize the fixed point of the LCO. However, given frequent sawtooth heat pulses, an I-phase can be driven. This occurs when the damping time of the oscillation is longer than the period of the sawtooth, i.e., $\gamma_{\text{oscillation}} < f_{\text{sawtooth}}$. Experiments using repetitive pulsed electron cyclotron heating (ECH) to control ELM activity are being pursued.³¹ Thus, it would be very interesting to explore the possibility of achieving a sustained I-phase using pulsed ECH.

V. SUMMARY AND DISCUSSION

We have reported the critical results of model studies of stimulated L \rightarrow H transitions and compared the evolution of these to those of spontaneous transitions. We have modeled the use of pellet injection and SMBI to trigger the L \rightarrow H transition and to control the H \rightarrow L back transition. A reduced L \rightarrow H transition model has been developed to explore the effect of internal deposition with an ambient heating. By using internal deposition, we can achieve stimulated transitions for lower—*subcritical*—ambient heating than we achieve spontaneous transitions for. The principal results of this study are

- (i) Particle injection, i.e., internal fueling near the edge, can trigger a subcritical $L \rightarrow H$ transition.
- (ii) The key effect caused by injection is a change of edge mean flow shear $\delta\langle V_E \rangle'$ induced by changes of density and temperature gradients. The density gradient peaks at the edge during injection, while the temperature profile softens at the edge.
- (iii) Edge mean shear $\langle V_E \rangle'$ is shown to be critical to turbulence collapse and the injection-induced transition.
- (iv) The injection-induced transition is sensitive to the number of particles injected per unit time, the location of deposition, and the degree of heating below the threshold.
- (v) Strong injection is shown to trigger a transient subcritical turbulence collapse. Repetitive injection at a period less than the lifetime of the collapsed state can maintain the subcritically collapsed state, leading to a driven, or “stimulated” H-mode.
- (vi) The total number of particles required to induce a transition by either injection or gas puffing is estimated. The total number injected particles is significantly smaller than that added by gas puffing. A change in edge profiles and $\langle V_E \rangle'$ is seen to be critical to the transition, i.e., we have shown that internal injection is more effective than gas puffing of comparable strength, at triggering transitions.
- (vii) Model studies suggest that the critical I_{SMBI} for triggering the $L \rightarrow H$ transition should increase with dQ . This resembles results for threshold dependence upon heat avalanche noise, distribution, i.e., $(\langle \sigma^2 \rangle$ vs dQ), and heat pulse size.
- (viii) Bursty or oscillatory behavior of zonal flows is not evident for injection-induced transition. Peaks in time of $R_T = \alpha_0 E_0 / (\gamma_L - \Delta\omega I)$ and $R_H = \alpha_V E_V / (\gamma_L - \Delta\omega I)$ coincide in the case of stimulated transitions, suggesting there is no causal link between zonal and mean flows for seen injection-induced transitions. This is in contrast to spontaneous transitions, where the peak in R_T leads the peak in R_H , and thus initiates the turbulence suppression. This finding suggests that there can be multiple pathways to the transition and that not all such pathways involve the same mechanism.
- (ix) Apart from the addition of internal fueling related terms, the model used here is identical to that used for studies of spontaneous transitions.

Naturally, we ask how do these results fit into our understanding of the $L \rightarrow H$ transition? Several years of intense research, world wide, have developed an emerging understanding of the standard, spontaneous transition. That is, when heat flux increases, a strong zonal flow is sufficiently excited, leading to I-phase oscillations or a single burst. When the zonal flow is excited, turbulence is reduced, allowing ∇p_i to steepen. Then, mean flow shear $\langle V_E \rangle'$ increases to lock in the H-mode. However, the key findings in injection-induced transitions are (i) a change of edge mean flow shear $\delta\langle V_E \rangle'$ is critical and can be achieved *directly*. (ii) Zonal flow production does not exhibit any sign of a peak or burst in advance of the transition, i.e., there is no peak in R_T prior

to the peak in $\langle V_E \rangle'$. (iii) $L \rightarrow H$ transitions can be achieved below the power threshold.

So, how do we reconcile the apparent difference in the evolution of stimulated and spontaneous transitions? It is illuminating to illustrate stimulated and spontaneous transitions in the space of heating power and fueling depth. Both transitions consist of heating and fueling, but are quite different in the distributions of heating and fueling, as illustrated in Fig. 11. The stimulated transition and spontaneous transitions take fundamentally different routes to achieve transport and profile bifurcations. The spontaneous transition achieves the transition via zonal flow excitation, to reduce turbulence and steepen ∇p_i . The steepened ∇p_i and increased $\langle V_E \rangle'$ spontaneously locks in the H-mode. The external injection of the stimulated transition directly steepens edge $\langle V_E \rangle'$ and ∇p_i . The directly enhanced edge $\langle V_E \rangle'$ immediately quenches turbulence. Though these routes to transition look different, increased edge $\langle V_E \rangle'$ locks in to the H-mode in the both cases. *The difference between the two transitions lies in how the state enhanced edge $\langle V_E \rangle'$ is achieved.*

These numerical studies are given by a simple reduced model with some specific sets of coefficients. The coefficients in this mean field model are determined by the underlying primitive equations. Universality classes for the model coefficients are discussed in Ref. 32. In order to make the physics of the stimulated transition clearer, further exhaustive comparisons with results of first-principles simulations and/or analyses from experiments are required in future work.

Key future tests for stimulated transitions are

- i) A *quantitative* comparison of SMBI and gas puff transition efficiencies would be illuminating. We have done this comparison in the course of this model study. A similar quantitative comparison in experiment would be of great interest.
- ii) Exploring analogous stimulated transitions, using heating, i.e., to explore near-edge pulsed heating to achieve and maintain transition would be interesting.³¹ Both SMBI and ECH have been used for ELM control. ECH excites ∇T , while SMBI excites ∇n . Thus, a study of the effect of edge ECH micropulsations in the $L \rightarrow H$ transitions is a natural complement to the SMBI study desired in this paper.

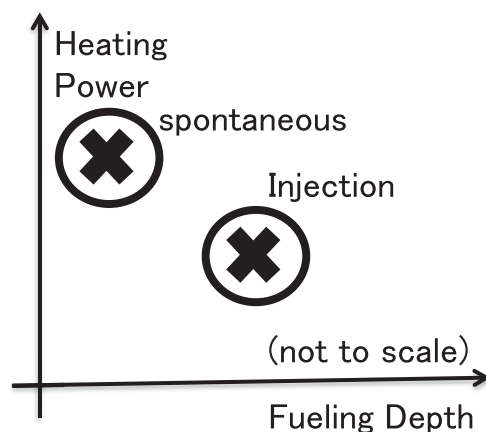


FIG. 11. Cartoon of stimulated (injection) and spontaneous transitions in the space of heating power and fueling depth. This diagram is not to scale.

iii) Can locally enhanced electron-ion coupling trigger transitions at low density?

In a spontaneous transition, $R_T = \langle \tilde{v}_r \tilde{v}_\theta \rangle \partial_r V_{ZF} / \gamma_{\text{eff}} \mathcal{E}$ at zonal flow peak is the key, however both turbulence collapse and transition initiate at the edge. In the stimulated transition, edge $\delta \langle V_E \rangle'$ is the key. How do we relate zonal flow evolution in the edge layer to mean shear at the separatrix? Spontaneous transition are initiated when the peak of zonal flow is close to the edge (i.e., within a turbulence correlation length.)

Some important open questions follow: What is the impact of toroidal rotation on stimulated transitions? Can we directly predict critical edge $\delta \langle V_E \rangle'$ for transition? When or how does the simple model of injection used here fail? Are predicted off-edge transitions with strong SMBI physical?

We also offer thoughts on future experiments. Can experiments deduce evolution of the edge $\langle V_E \rangle'$ enhancement as functions of I_{SMBI} , pellet penetration, and pulse length relationship? Can they study flow (zonal and mean) during injection-induced transition with weakly enhanced gas puffing? In particular, measuring $\langle \tilde{v}_r \tilde{v}_\theta \rangle \partial_r V_{ZF} / \gamma_{\text{eff}} \mathcal{E}$ dynamics would be interesting. Can experiments verify the predicted enhanced hysteresis? Can they confirm the existence of a “transient” H-state? Can they sustain the H-mode via repetitive pulsed injection? Investigation of the repetition rate f_{SMBI} sensitivity and the range of dQ would be interesting. We note that experimentalists should perform studies at n_0 above minimum power threshold $P_T(n_0)$, to avoid the triviality of $dP_T/dn < 0$ with $\delta n > 0$.

ACKNOWLEDGMENTS

The authors thank P. T. Lang and H. Zohm for a very stimulating discussion as to comparing injection and gas puffing. We also thank P. Gohil, G. McKee, L. Schmitz, F. Ryter, T. Estrada, C. Hidalgo, K. J. Zhao, M. Xu, J. Q. Dong, B. Duval, and N. Fedorczak for discussions. This work was supported by the WCI Program of the National Research Foundation of Korea funded by the Ministry of Education, Science and Technology of Korea [WCI 2009-001] and the Department of Energy under Award Number DE-FG02-04ER54738 and CMTFO.

¹H. Mori and Y. Kuramoto, *Dissipative Structures and Chaos* (Springer-Verlag, Berlin, 1998).

²R. A. Fisher, *Annu. Eugen.* **7**, 355 (1937).

³A. Kolmogorov, I. Petrovsky, and N. Piscounoff, *Bull. Moskov Gos. Univ.* **A1**, 1 (1937).

⁴B. P. Belousov, in *Oscillations and Traveling Waves in Chemical Systems*, edited by R. Field and M. Burger (John Wiley, New York, 1985), pp. 605–613.

⁵F. Wagner, G. Becker, K. Behringer, D. Campbell, A. Eberhagen, W. Engelhardt, G. Fussmann, O. Gehre, J. Gernhardt, G. v. Gierke, G. Haas, M. Huang, F. Karger, M. Keilhacker, O. Klüber, M. Kornber, K. Lackner, G. Lisitano, G. G. Lister, H. M. Mayer, D. Meisel, E. R. Müller, H. Murmann, H. Niedermeyer, W. Poschenrieder, H. Rapp, H. Röhr, F. Schneider, G. Siller, E. Speth, A. Stäbler, K. H. Steuer, G. Venus, O. Vollmer, and Z. Yü, *Phys. Rev. Lett.* **49**, 1408 (1982).

⁶C. Gormezano, A. C. C. Sips, T. C. Luce, S. Ide, A. Becoulet, X. Litaudon, A. Isayama, J. Hobbirk, M. R. Wade, T. Oikawa et al., *Nucl. Fusion* **47**, S285 (2007).

⁷P. H. Diamond, S.-I. Itoh, K. Itoh, and T. S. Hahn, *Plasma Phys. Controlled Fusion* **47**, R35 (2005).

⁸T. Estrada, T. Happel, C. Hidalgo, E. Ascasibar, and E. Blanco, *EPL* **92**, 35001 (2010).

⁹G. S. Xu, B. N. Wan, H. Q. Wang, H. Y. Guo, H. L. Zhao, A. D. Liu, V. Naulin, P. H. Diamond, G. R. Tynan, M. Xu, R. Chen, M. Jiang, P. Liu, N. Yan, W. Zhang, L. Wang, S. C. Liu, and S. Y. Ding, *Phys. Rev. Lett.* **107**, 125001 (2011).

¹⁰L. Schmitz, L. Zeng, T. L. Rhodes, J. C. Hillesheim, E. J. Doyle, R. J. Groebner, W. A. Peebles, K. H. Burrell, and G. Wang, *Phys. Rev. Lett.* **108**, 155002 (2012).

¹¹T. Estrada, C. Hidalgo, T. Happel, and P. H. Diamond, *Phys. Rev. Lett.* **107**, 245004 (2011).

¹²K. Miki, P. H. Diamond, O. D. Gurcan, G. R. Tynan, T. Estrada, L. Schmitz, and G. S. Xu, *Phys. Plasmas* **19**, 092306 (2012).

¹³Y. R. Martin, T. Takizuka, and the ITPA CDBM H-mode Threshold Database Working Group, *J. Phys.: Conf. Ser.* **123**, 012033 (2008).

¹⁴F. Ryter, T. Pütterich, M. Reich, A. Scarabosio, E. Wolftrum, R. Fischer, M. G. Adamov, N. Hicks, B. Kurzan, C. Maggi, R. Neu, V. Rohde, G. Tardini, and the ASDEX Upgrade TEAM, *Nucl. Fusion* **49**, 062003 (2009).

¹⁵K. Miki, P. H. Diamond, L. Schmitz, D. C. McDonald, T. Estrada, O. D. Gurcan, and G. R. Tynan, *Phys. Plasmas* **20**, 062304 (2013).

¹⁶P. Manz, G. S. Xu, B. N. Wan, H. Q. Wang, H. Y. Guo, I. Cziegler, N. Fedorczak, C. Holland, S. H. Müller, S. C. Thakur, M. Xu, K. Miki, P. H. Diamond, and G. R. Tynan, *Phys. Plasmas* **19**, 072311 (2012).

¹⁷W. Fundamenski, F. Militello, D. Moulton, and D. McDonald, *Nucl. Fusion* **52**, 062003 (2012).

¹⁸L. G. Askinazi, V. E. Golant, S. V. Lebedev, L. S. Levin, V. A. Rozhansky, and M. Tendler, *Phys. Fluids B* **5**, 2420 (1993).

¹⁹P. Gohil, L. R. Baylor, T. C. Jernigan, K. H. Burrell, and T. N. Carlstrom, *Phys. Rev. Lett.* **86**, 644 (2001).

²⁰P. Gohil, L. R. Baylor, K. H. Burrell, T. A. Casper, E. J. Doyle, C. M. Greenfield, T. C. Jernigan, J. E. Kinsey, C. J. Lasnier, R. A. Moyer, M. Murakami, T. L. Rhodes, D. L. Rudakov, G. M. Staebler, G. Wang, J. G. Watkins, W. P. West, and L. Zeng, *Plasma Phys. Controlled Fusion* **45**, 601 (2003).

²¹X. R. Duan, J. Q. Dong, L. W. Yan, X. T. Ding, Q. W. Yang, J. Rao, D. Q. Liu, W. M. Xuan, L. Y. Chen, X. D. Li, G. J. Lei, J. Y. Cao, Z. Cao, X. M. Song, Y. Huang, Y. Liu, W. C. Mao, Q. M. Wang, Z. Y. Cui, X. Q. Ji, B. Li, G. S. Li, H. J. Li, C. W. Luo, Y. Q. Wang, L. H. Yao, L. Y. Yao, J. H. Zhang, J. Zhou, Y. Zhou, Y. Liu, and the HL-2A team, *Nucl. Fusion* **50**, 095011 (2010).

²²H.-J. Sun, X.-T. Ding, L.-H. Yao, B.-B. Feng, Z.-T. Liu, X.-R. Duan, and Q.-W. Yang, *Plasma Phys. Controlled Fusion* **52**, 045003 (2010).

²³W. W. Xiao, P. H. Diamond, X. L. Zou, J. Q. Dong, X. T. Ding, L. H. Yao, B. B. Feng, C. Y. Chen, W. L. Zhong, M. Xu, B. S. Yuan, T. Rhee, J. M. Kwon, Z. B. Shi, J. Rao, G. J. Lei, J. Y. Cao, J. Zhou, M. Huang, D. L. Yu, Y. Huang, K. J. Zhao, Z. Y. Cui, X. M. Song, Y. D. Gao, Y. P. Zhang, J. Cheng, X. Y. Han, Y. Zhou, Y. B. Dong, X. Q. Ji, Q. W. Yang, Y. Liu, L. W. Yan, X. R. Duan, Y. Liu, and the HL-2A Team, *Nucl. Fusion* **52**, 114027 (2012).

²⁴K. Miki, P. H. Diamond, S. H. Hahn, W. W. Xiao, O. D. Gurcan, and G. R. Tynan, *Phys. Rev. Lett.* **110**, 195002 (2013).

²⁵E.-J. Kim and P. H. Diamond, *Phys. Rev. Lett.* **90**, 185006 (2003).

²⁶K. Miki, P. H. Diamond, N. Fedorczak, O. D. Gurcan, M. Malkov, C. Lee, Y. Kosuga, G. R. Tynan, G. S. Xu, T. Estrada, D. C. McDonald, L. Schmitz, and K. J. Zhao, *Nucl. Fusion* **53**, 073044 (2013).

²⁷N. Fedorczak, P. Diamond, G. Tynan, and P. Manz, *Nucl. Fusion* **52**, 103013 (2012).

²⁸T. Estrada, C. Hidalgo, and T. Happel, *Nucl. Fusion* **51**, 032001 (2011).

²⁹F. Wagner, G. Fussmann, T. Grave, M. Keilhacker, M. Kornherr, K. Lackner, K. McCormick, E. R. Müller, A. Stäbler, G. Becker, K. Bernhardt, U. Ditte, A. Eberhagen, O. Gehre, J. Gernhardt, G. v. Gierke, E. Glock, O. Gruber, G. Haas, M. Hesse, G. Janeschitz, F. Karger, S. Kissel, O. Klüber, G. Lisitano, H. M. Mayer, D. Meisel, V. Mertens, H. Murmann, W. Poschenrieder, H. Rapp, H. Röhr, F. Ryter, F. Schneider, G. Siller, P. Smeulders, F. Söldner, E. Speth, K. H. Steuer, Z. Szymanski, and O. Vollmer, *Phys. Rev. Lett.* **53**, 1453 (1984).

³⁰K. J. Zhao et al., in *Proc. 24th Int. Conf. Fusion Energy 2012 San Diego* (2012), IAEA-CN-197/EX/7-2Ra.

³¹B. Duval et al., in *Proceedings of the 24th IAEA Fusion Energy Conf., San Diego, USA* (2012), IAEA-CN-197/EX/1-2.

³²P. H. Diamond, Y. M. Liang, B. A. Carreras, and P. W. Terry, *Phys. Rev. Lett.* **72**, 2565 (1994).